Optical coherence tomography for process control of laser micromachining

Markus Wiesner,[1] Jürgen Ihlemann,[1] Heike H. Müller,[2] Eva Lankenau,[2] and Gereon Hüttmann[2]
[1]*Laser-Laboratorium Göttingen e.V., Hans-Adolf-Krebs-Weg 1, D-37077 Göttingen, Germany*
[2]*Institute of Biomedical Optics, University of Lübeck, Peter-Monnik-Weg 4, D-23562 Lübeck, Germany*

(Received 2 November 2009; accepted 15 February 2010; published online 24 March 2010)

In situ surface imaging for nondestructive evaluation (NDE) by optical coherence tomography (OCT) before, during, and after ablative laser processing is presented. Furthermore, it is shown that the ability of *in situ* characterization is beneficial for samples such as optical fibers, which are difficult to handle in the standard analysis. Surface images taken by the OCT are compared with these common analysis tools such as scanning electron microscopy (SEM), reflected-light, and confocal microscopy. An axial resolution of ~126 nm for surface detection and a lateral resolution <2.5 μm are obtained and the potential of the setup to imaging structures with high aspect ratio is demonstrated. © *2010 American Institute of Physics.* [doi:10.1063/1.3356080]

I. INTRODUCTION

High resolution laser micromachining is a demanding application for positioning and alignment systems. It requires careful adjustment of the sample and online controlling of parameters such as ablation rate and focus position. Nondestructive testing and evaluation (NDT/NDE) is an important part of the laser process and of the quality management in general. *Ex situ* characterization of the machined work piece with the need of subsequent readjustment into the processing system are time consuming and hold the risk of contaminating and damaging the microstructure. In this paper, we will present a concept to solve these problems by the integration of an optical coherence tomography (OCT) module for *in situ* control into an existing F_2-laser microprocessing system.

OCT is a recently introduced method for nondestructive, noncontact, and multidimensional visualization, with many applications in the investigation of biomedical specimens, especially in the area of ophthalmology.[1] The method has been under constant development since its introduction in the year 1991.[2] It achieves high resolution imaging on the micron level with a high sensitivity and a large dynamic range by the interferometric detection of backscattered and reflected light from structures and interfaces in the sample.[3]

Based on the principle of white-light interferometry, the most common OCT setup is a Michelson interferometer illuminated by a temporally low-coherence light source. Mainly near-infrared light sources are used to penetrate the surface of opaque or turbid materials by some millimeters to yield depth information. A depth scan (A-scan) of the reference mirror provides interference between the sample and reference beams and a depth-resolved reflectivity profile is obtained. By deflecting the sample beam with a xy-scanner, cross-sectional (B-scans), or three-dimensional (3D) imaging is possible.

Besides the traditional time-domain OCT[4] new techniques have been developed and established to enhance performance and imaging quality. Spectral-domain (SD-)OCT[5,6] and swept-source (SS-)OCT[7] lead to improved sensitivity[8–10] and imaging speed. Scan rates up to 568 600 A-scans/s for SS-OCT[11] and 312 500 A-scans/s for SD-OCT[12] have been realized, which enables real-time monitoring. Supported by improved light sources ultrahigh resolution (UHR-)OCT with depth resolutions down to 1 μm and superior imaging quality becomes available.[13,14] High resolution imaging combined with new contrast mechanisms is often required for many applications in materials research because in many cases structures with sizes of a few microns are relevant.

In recent years, applications for nonmedical purposes have become interesting and now find their way into industrial use.[15,16] Implementations can be found in the field of optical metrology[17] and noncontact material characterization. The decoupling of lateral and axial resolution allows the measurement of structures with a high aspect ratio like bore holes.[18] The determination of the refractive index[19] is also possible as well as measurements of thickness[20] and distances[21] or the survey of roughness of a specimen's surface.[22,23]

A more sophisticated utilization of OCT is the combination with established measurement and manufacturing processes such as laser-induced breakdown spectrometry to provide additional ablation depth information for spectrometric analysis[24] or high speed *in situ* cross-sectional depth profiling of ultrafast micromachining by using one light source for both imaging and machining.[25] Process control with OCT in general has been reported to supplement manufacturing[26] or to replace sensors in harsh conditions to enhance measurement precision.[21] Recently, imaging rates were presented, which allow investigating the temporal dynamics of the laser ablation process itself.[27] The introduction of so called functional OCT has added more aspects to this field of applications. Spectroscopic analysis,[28] flow characterization[29] for microfluidics, and evaluation of strain fields[30] are just a few examples.

Hence, one of the largest fields of industrial utilization

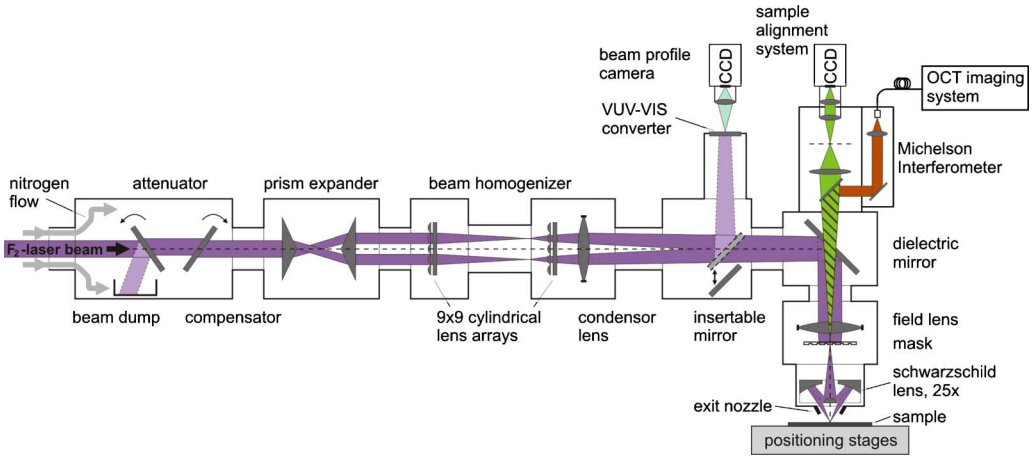

FIG. 1. (Color online) High resolution Schwarzschild configuration of the F_2-laser optical processing system with OCT add on.

so far can be found in NDT/NDE. Imaging and characterization of laser-induced damage sites in optical components[31] or the investigation of different polymers, ceramics, and composite materials[32,33] have been reported.

However, for material investigations many applications demand the visualization of the whole sample surface, which cannot obtained by point (A-scan) or cross-sectional (B-scan) measurements. Thus transversal (en-face) scanning is needed to yield the essential information.[34,35] It has been shown that this technique is capable to outperform imaging methods that rely solely on the confocal principle.[36] In general, noncontact process control for high resolution laser micromachining can be fulfilled by many optical techniques, e.g., fringe projection, triangulation, confocal microscopy, or interferometry. Of all optical methods, the white light interferometry is distinguished by the fact that the accuracy with which a surface can be determined does not depend on the aperture, i.e., the focusing angle of the incident radiation to the surface.[37] In addition, the use of a SD-OCT makes mechanical scanning of the sample in z direction unnecessary and keeps the mechanical complexity moderate. Therefore, fast and high precision surface detection, even with large working distance, limited space, and within structures with high aspect ratio can be achieved. Especially the comparatively simple integration into established measurement and manufacturing processes seems a promising way to establish new techniques and shows the versatile capabilities of OCT for industrial applications. In particular, high precision laser processing methods such as ablation, pattering, or 3D micromachining can benefit from this kind of process control. This paper will present the integration of a UHR-SD-OCT with the ability of surface imaging into an existing F_2-laser processing system. Possible applications such as NDT of micromachined surfaces or alignment purposes will be shown.

II. OPTICAL SYSTEM AND SETUP

The F_2-laser processing system consists of a F_2-laser (Lambda Physik LPF 220i), a 157 nm beam-shaping and -delivery system (MicroLas Lasersystem), high precision target positioning drives, and beam and sample-alignment diagnostics. It has been described in detail previously.[38] Ablative processing of materials is performed in a mask projection configuration. The laser delivers up to 25 mJ single-pulse energy with 15 ns pulse duration at 1–200 Hz repetition rate. Homogenization and imaging optics are assembled in a 3 m long aluminum chamber, which is flushed with nitrogen gas to provide transparency at 157 nm. The mask is illuminated with the homogenized laser beam and imaged onto the work piece at 25× demagnification using a Schwarzschild objective of 0.4 numerical aperture (NA). The optical system provides a uniformly illuminated target field of size 240×240 μm^2. The target sample is positioned outside the chamber on a high precision translation stage. A gas flow nozzle separates the imaging optics from the sample to provide a protective and transparent stream of nitrogen gas to the working area on the target surface [Fig. 1]. With this setup, ablative machining even of transparent materials such as glass and quartz is possible, as the short wavelength of 157 nm serves for efficient absorption. Thus, high precision manufacturing of optical components such as submicron gratings[39] or microlenses on the end faces of optical fibers[40] has been demonstrated. Due to the short wavelength λ being used in combination with the high NA of the Schwarzschild objective the depth of field (DOF) is very limited. According to the well-known equation[41]

$$\mathrm{DOF} = \pm 0.5\frac{\lambda}{\mathrm{NA}^2}, \tag{1}$$

the DOF is about 1.0 μm. This must be taken into account during the alignment process to secure precise processing. In a basic version, the alignment of the image plane (z-alignment) is accomplished using the camera of the sample alignment system or by applying a test series of ablation spots with varying z to find the exact image plane. Both methods are time consuming and not very reliable, the latter is even damaging part of the work piece. Furthermore, online control of the sample position for longer manufacturing processes is not possible and the detection of tilted sample surfaces a major problem. For these reasons, a more sophisticated alignment and focus control method is needed. The adoption of the OCT ability for surface detection is implemented here to solve these problems. The OCT system consists of a commercial SD-OCT imaging system (Thorlabs

Inc.), including the data acquisition and the illumination, combined with a customized Michelson interferometer and a galvanometric scanner system. The OCT imaging system has an A-scan sample rate of 1.4 kHz and uses a superluminescent diode for illumination with an output power of 8.4 mW. The central wavelength is $\lambda_0 = 926.3$ nm with a full width at half maximum bandwidth of $\Delta\lambda = 95.1$ nm. The axial resolution Δz of the OCT systems can be described by[42]

$$\Delta z = \frac{l_c}{2} = \frac{2 \ln 2}{\pi} \frac{\lambda_0^2}{\Delta\lambda} \tag{2}$$

and depends on the coherence length l_c of the light source. Since SD-OCT acquires a depth-resolved reflectivity profile with a single A-scan, the maximum scanning depth $z_{\max}$ is determined by[42]

$$z_{\max} = \frac{1}{4n} \frac{\lambda_0^2}{\Delta\lambda} N, \tag{3}$$

where n is the sample's refractive index and N is the number of spectrometer detector elements. According to this equation, the maximum scanning depth scales linearly with the number of detector elements. With $N = 1024$ the theoretical measurement depth of our OCT system is $z_{\max} = 2.3$ mm with an axial resolution of $\Delta z = 3.9$ μm.

An obvious advantage of OCT is that the axial and lateral resolutions are decoupled, so that it is possible to optimize the system design for lateral scanning without affecting the axial resolution. The lateral resolution itself depends on the optical constraint of the sample arm optics and is described by the resolution limit for image formation in microscopes[41]

$$\Delta x = 0.61 \frac{\lambda}{\mathrm{NA}}. \tag{4}$$

In our case, the OCT uses the same Schwarzschild type reflective objective that is used for the laser processing beam. This is possible due to the broadband reflective coating and the achromatic nature of this optics device. The 0.4 NA of the Schwarzschild objective provides a lateral resolution of $\Delta x = 1.4$ μm at the OCT wavelength and, according to Eq. (1) a DOF of 5.8 μm. For defining the position of a surface, the measured OCT peak was fitted with a parabolic function and the exact position of the maximum was determined. With optical smooth surfaces, the measurement precision was limited by mechanical vibration and with optically scattering surfaces the accuracy was reduced due to speckle formation.

The setup and beam path of the Michelson interferometer is shown in Fig. 2. The emitted light is guided from the imaging system by a single mode fiber to the Michelson interferometer and split into the reference and sample arms. The reference arm is folded twice to keep the setup as compact as possible. The integration of the OCT through the existing sample alignment system makes *in situ* monitoring of the target field and the mask possible. For coupling the OCT beam path into the sample alignment beam path, a cube beam splitter was integrated under the illumination port of the sample alignment. After that the OCT beam path is identical to the sample alignment beam path, passes the field lens

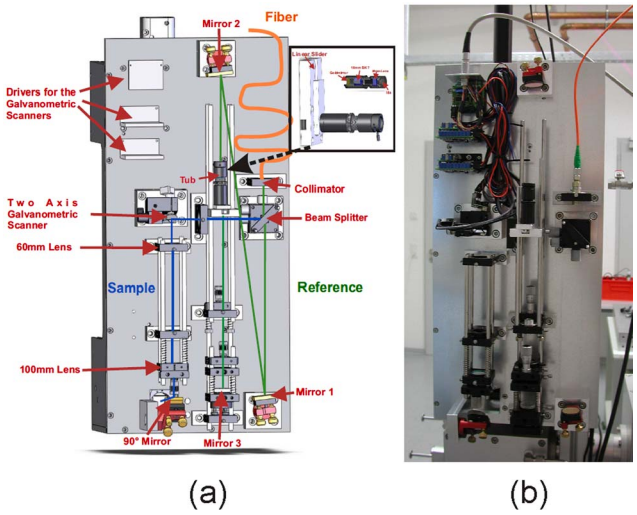

FIG. 2. (Color online) (a) Configuration and (b) photographic views of the customized Michelson interferometer at the backside of the sample alignment system.

of the F_2-laser optical processing system, and is focused into the mask plane. From there, the focus spot is imaged by the Schwarzschild objective onto the target field. The sample arm optics were customized so that it meets the necessary optical conditions for monitoring the target field of both the Schwarzschild objective and the mask. For monitoring the mask plane, it is required to match the shorter sample arm by swing a mirror tub into the reference arm.

For surface scans, the sample arm can be deflected by a galvo scanner system (6210H, Cambridge Technology, USA). The scanner system allows us to scan the whole target field (240×240 μm^2) of the F_2-laser processing system with a maximum number of 542×542 A-scans for one image. In principle, it is possible to scan the whole Schwarzschild objective field of view of 720 μm, but the empty mask holder restricts the maximum scanning field to 300×300 μm^2.

III. SYSTEM PERFORMANCE

Main purpose of the installed OCT is the *in situ* surface detection and imaging for alignment purposes and NDE before, during, and after laser processing. We demonstrate here the potential of the setup to imaging structures with high aspect ratio, which are not accessible for most common analyze tools such as confocal microscopy or scanning electron microscopy (SEM). Furthermore, it is shown that the ability of *in situ* characterization is beneficial for samples which are difficult to handle in the standard analysis such as optical fibers, which may be too long and bulky for investigation under a microscope or SEM. In particular, SEM is restricted to spot test or the inspection of prototypes because of the contamination by the required metal coating.

A. Surface inspection

Figure 3 shows a SEM image of a line grating on the end face of a 400 μm multimode optical fiber which was manufactured by the F_2-laser processing system. Due to the large size of the grating, ablation of each line by a slit mask was

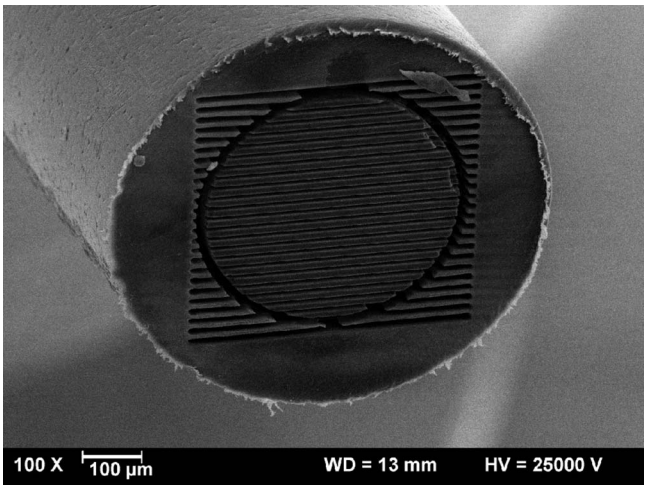

FIG. 3. SEM image of 20 μm line grating at the end face of a 400 μm multimode optical fiber.

not possible, so each line was written by imaging a spot on the surface and then moving the fiber relative to the laser with a velocity of 14 μm/s. The laser was triggered with 50 Hz and the fluence was about 6.8 J/cm^2. The slightly damaged area of the line grating in the upper right was investigated by the OCT to demonstrate the ability of detecting small damage sites within NDT. The scan area is 200×200 μm^2 and consists of 400×400 A-scans [Fig. 4(a)]. Figure 4(b) provides a closer look of the structure. The scan area is 80×80 μm^2 consisting of 540×540 A-scans. The different ablation depth for the coating, cladding, and the fused silica core, as a result of the different ablation rates are recognizable [Fig. 4(c)]. The grating period is 20 μm

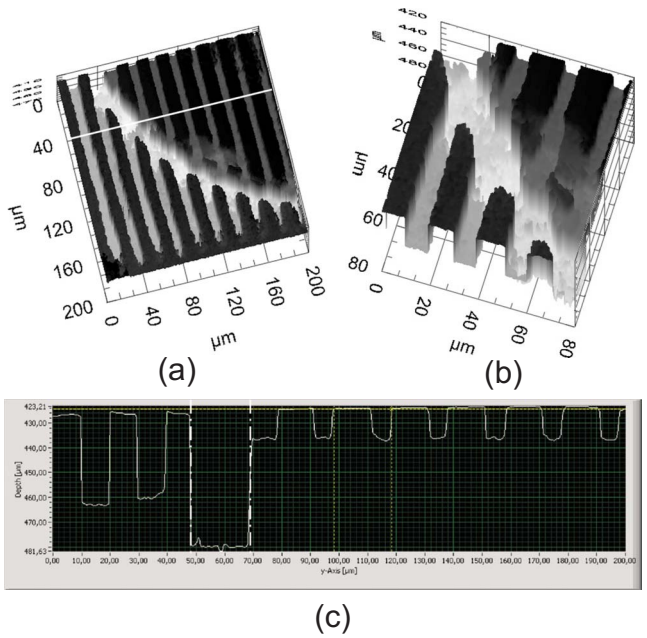

FIG. 4. (Color online) (a) Surface image of the fiber end face (cf. Fig. 3) showing an area of 200×200 μm^2. Thin white line indicates where the B-scan was obtained. (b) In this image, the scan area was reduced to 80×80 μm^2 consisting of 540×540 A-scans. In both images, the damaged area is clearly visible. (c) B-scans show the different ablation depth for the coating (left), cladding (middle) and the fused silica core (right), separated by the dotted lines.

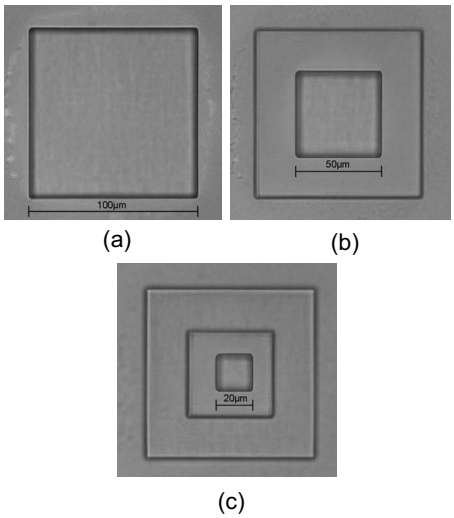

FIG. 5. Three step manufacturing of a simple "stepped pyramid." Between each step the sample was released from its holder and the microscopic image was taken. After realignment, the next step was applied. This example shows the reliability of the OCT alignment capabilities. After the ablation, the measured depth via A-scan in the middle of the structure was (a) 2.1 μm, (b) 4.8 μm, (c) 8 μm.

with a gap width of 7 μm and covers the whole core of the fiber. The depth of the structure is about 13 μm at the core area. The aforementioned cracks are also clearly visible [Figs. 4(a) and 4(b)].

B. Work piece alignment

OCT is not limited to inspection purposes, also work piece alignment is feasible. It is possible to even remove the specimen from its holder and to realign it within the optical system with the help of the OCT.

Figures 5(a)–5(c) shows a simple "stepped pyramid" structure, which was ablated in a three step process, by reducing the lateral length of a square mask (2.5, 1.25, and 0.5 mm) inserted in the mask plane for every ablation step. First, the surface was detected by the OCT and moved to the image plane of the Schwarzschild objective. A square aperture mask with a lateral length of 2.5 mm was used for the ablation. Sixteen pulses with a fluence of 4 J/cm^2 were applied, so that a square was ablated in the material. An A-scan by the OCT at the center of the structure delivered a depth of ~2.1 μm. The sample was released from the holder and investigated under a reflected-light microscope [Fig. 5(a)]. The sample was then replaced to the holder and realigned by the OCT. For the next step, the lateral size of the square aperture mask was reduced to 1.25 mm and the abovementioned ablation was applied again. The structure depth measured by the OCT at the center was now 4.8 μm. A third step with a lateral mask size of 0.5 mm was performed and resulted in a final depth of 8 μm at the center of the structure. Figure 5(a)–5(c) shows that realignment of the sample was successful and every ablated structure has sharp boundaries. A comparison with depth measurements taken by a confocal microscope (Sensofar Plu 2300) after the end of manufacturing are shown in Table I.

TABLE I. Comparison of depth measurements by OCT and a commercial confocal microscope.

	OCT (μm)	Confocal microscope (μm)
Step 1	2.1	2.4
Step 2	4.8	5.0
Step 3	8.0	7.8

A surface image of a more suitable pyramid structure was taken to demonstrate the capability to detect debris which is produced during the manufacturing process. Comparison between the reflected-light microscopic and the OCT images shows that the debris deposited around the topmost square could be clearly resolved by the OCT [Figs. 6(a) and 6(b)]. Furthermore the roughness induced by the F_2-laser ablation on the surface of the micromachined structure[43] can be detected by the OCT [Figs. 6(c) and 6(d)].

C. Resolution

To evaluate the performance of our measurement system, we used a lithographically manufactured phase mask. This four-step phase mask was well characterized[44] and used for beam shaping of partial coherent UV laser beams. Every step has a height of 126 ± 3 nm with a lateral pixel size of 2.5 μm. Figures 7(a) and 7(b) shows surface images taken with the OCT. The picture (a) shows an area of 150×150 μm^2 consisting of 300×300 A-scans. The different heights of the steps are well-defined and gray-scale resolved. By reducing the scan area to 50×50 μm^2, also with 300×300 A-scans, not only the individual pixels can be clearly distinguished, it also makes defects smaller than the pixel size of 2.5 μm visible [Fig. 7(b)]. For comparison purposes, pictures taken by SEM and a reflected-light microscope are shown in Fig. 7(c) and 7(d). For defining the position z_S of a surface, the measured OCT peak was fitted with a parabolic function by

$$z_S = z_p + \frac{I_{p-1} - I_{p+1}}{(I_{p-1} + I_{p+1} - 2 \cdot I_p)} \cdot \frac{1}{2}, \tag{5}$$

where z_p and I_p are the coordinates of the maximum value and the proximate values I_{p-1} and I_{p+1}. Figure 8 shows exemplary the parabolic fitting to the OCT data for two surface points at nearby pixels with different step heights. The difference of these two points is the step height. In this example, we found a height difference of $\Delta z_S = 0.125$ μm.

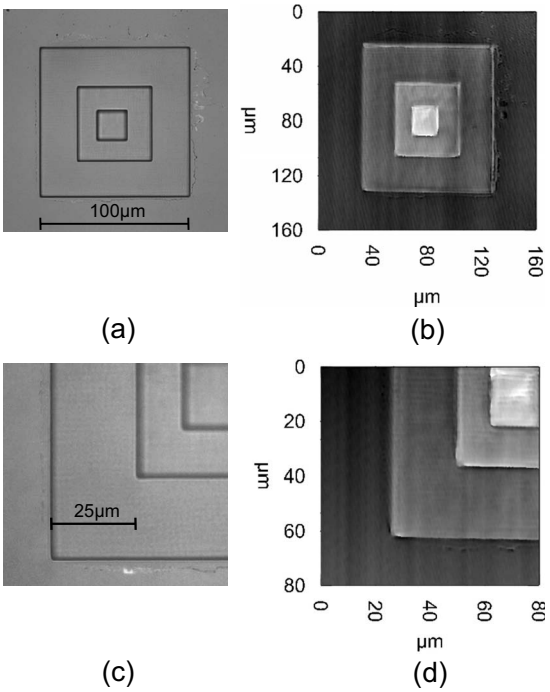

FIG. 6. Comparison between reflected-light microscope and surface OCT images. (a) 500× magnification of the microstructure and (b) matchable OCT presentation with 400×400 A-scans. The debris around the structure is resolved in both images. Furthermore the OCT image contains grayscale encoded height information. By increasing the magnification to 1000× (c) and reducing the scan area from 160×160 to 80×80 μm^2 (d) the roughness of the surface becomes visible.

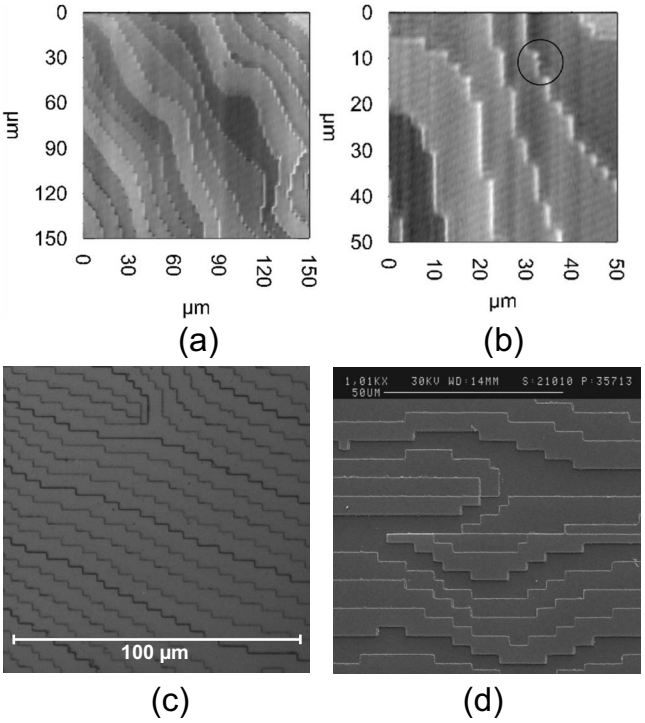

FIG. 7. Surface OCT images of the phase mask with the size of 150×150 μm^2 (a) and 50×50 μm^2 (b). Defect (circle) smaller than 2.5 μm can be also seen in the upper right of (b). Both images consist of 300×300 A-scans. For comparison images were also taken with a reflected-light microscope (c) and a SEM (d).

IV. CONCLUSION

We have presented an implementation of an UHR-SD-OCT into an existing F_2-laser processing system for *in situ* NDE of micromachined surfaces and alignment purposes. We compared the surface images taken by the OCT with common analysis tools such as SEM, reflected-light, and confocal microscopy. The results show that it is possible to use OCT for surface detection and imaging in the field of laser micromachining. Furthermore reliable focusing and tilt

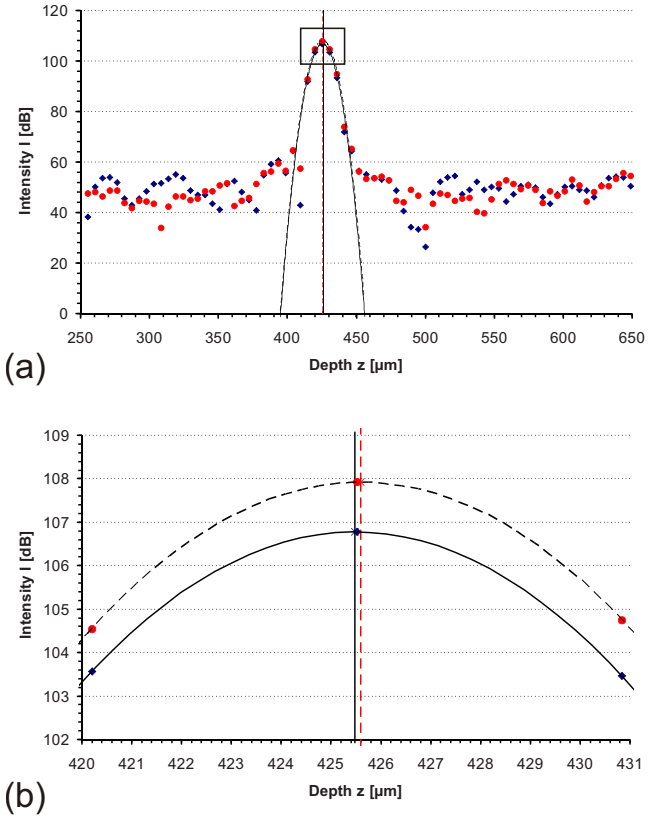

FIG. 8. (Color online) Parabolic fit to the OCT data for two different surface points of the phase mask (red dots and blue diamonds). (a) Overview of the parabolic fit to the found OCT peak. (b) Enlargement of the peak to show the different position of the two vertexes. The difference of these two points is step height of two pixel structures.

detection of the sample within the alignment process is possible. Multistep ablation with intermediate removal of the sample becomes possible. An axial resolution of ~126 nm for surface detection and a lateral resolution <2.5 μm were obtained. Unfortunately, the low scanning rate of 1.4 kHz for A-scans makes high resolution imaging time consuming. Here, further improvement of the current setup is needed. Scanning rates up to 200 kHz are desirable. With proper synchronization to the F_2-laser processing system online measurement of the ablation rate or investigation of the temporal dynamics of the laser ablation process itself should be possible. Especially for industrial application a more compact and rugged setup without fiber guidance is needed. On balance, the OCT has proven to be versatile for both surface imaging and sample alignment. The integration into the F_2-laser processing system has already reduced processing time, rejection rate, and enhanced the whole manufacturing process itself by the capability of *in situ* NDE.

ACKNOWLEDGMENTS

We would like to thank Jörg Meinertz, Tim Bonin and the Thorlabs HL AG for useful discussions and Markus Sailer for skilled SEM and confocal microscopy measurements. Financial support by the German Federal Ministry of Economics and Technology is gratefully acknowledged (Grant No. 16IN0351).

[1] M. Wojtkowski, R. Leitgeb, A. Kowalczyk, T. Bajraszewski, and A. F. Fercher, J. Biomed. Opt. **7**, 457 (2002).
[2] D. Huang, E. A. Swanson, C. P. Lin, J. S. Schuman, W. G. Stinson, W. Chang, M. R. Hee, T. Flotte, K. Gregory, C. A. Puliafito, and J. G. Fujimoto, Science **254**, 1178 (1991).
[3] A. F. Fercher, W. Drexler, C. K. Hitzenberger, and T. Lasser, Rep. Prog. Phys. **66**, 239 (2003).
[4] E. A. Swanson, D. Huang, M. R. Hee, J. G. Fujimoto, C. P. Lin, and C. A. Puliafito, Opt. Lett. **17**, 151 (1992).
[5] A. Fercher, C. Hitzenberger, G. Kamp, and S. El-Zaiat, Opt. Commun. **117**, 43 (1995).
[6] G. Häusler and M. W. Lindner, J. Biomed. Opt. **3**, 21 (1998).
[7] M. A. Choma, K. Hsu, and J. A. Izatt, J. Biomed. Opt. **10**, 044009 (2005).
[8] J. F. de Boer, B. Cense, B. H. Park, M. C. Pierce, G. J. Tearney, and B. E. Bouma, Opt. Lett. **28**, 2067 (2003).
[9] R. A. Leitgeb, C. K. Hitzenberger, and A. F. Fercher, Opt. Express **11**, 889 (2003).
[10] M. A. Choma, M. V. Sarunic, C. Yang, and J. A. Izatt, Opt. Express **11**, 2183 (2003).
[11] C. M. Eigenwillig, W. Wieser, B. R. Biedermann, and R. Huber, Opt. Lett. **34**, 725 (2009).
[12] B. Potsaid, I. Gorczynska, V. J. Srinivasan, Y. Chen, J. Jiang, A. Cable, and J. G. Fujimoto, Opt. Express **16**, 15149 (2008).
[13] M. Wojtkowski, V. J. Srinivasan, T. H. Ko, J. G. Fujimoto, A. Kowalczyk, and J. S. Duker, Opt. Express **12**, 2404 (2004).
[14] W. Drexler, U. Morgner, F. X. Kärtner, C. Pitris, S. A. Boppart, X. D. Li, E. P. Ippen, and J. G. Fujimoto, Opt. Lett. **24**, 1221 (1999).
[15] D. Stifter, Appl. Phys. B: Lasers Opt. **88**, 337 (2007).
[16] P. Targowski, M. Gora, and M. Wojtkowski, Laser Chem. **2006**, 35373 (2006).
[17] M. L. Dufour, G. Lamouche, V. Detalle, B. Gauthier, and P. Sammut, Insight **47**, 216 (2005).
[18] T. Dresel, G. Häusler, and H. Venzke, Appl. Opt. **31**, 919 (1992).
[19] G. J. Tearney, M. E. Brezinski, J. F. Southern, M. R. Hee, B. E. Bouma, and J. G. Fujimoto, Opt. Lett. **20**, 2258 (1995).
[20] M. Haruna, M. Ohmi, T. Mitsuyama, H. Tajiri, H. Maruyama, and M. Hashimoto, Opt. Lett. **23**, 966 (1998).
[21] L. Giniunas, R. Karkockas, and R. Danielius, Appl. Opt. **37**, 6729 (1998).
[22] P. Ettl, B. Schmidt, M. Schenk, I. Laszlo, and G. Häusler, Proc. SPIE **3407**, 133 (1998).
[23] M. M. Amarala, M. P. Raelea, J. P. Calyb, R. E. Samada, and A. Z. Freitasa, Proc. SPIE, **7390**, 73900Z (2009).
[24] E. A. Kwiatkowska, J. Marczak, R. Ostrowski, W. Skrzeczanowski, M. Sylwestrzak, M. Iwanicka, and P. Targowskia, Proc. SPIE **7391**, 73910F (2009).
[25] P. J. Webster, M. S. Muller, and J. M. Fraser, Opt. Express **15**, 14967 (2007).
[26] G. M. Guss, I. L. Bass, R. P. Hackel, C. Mailhiot, and S. G. Demos, Appl. Opt. **47**, 4569 (2008).
[27] W. Y. Oh, S. H. Yun, B. J. Vakoc, G. J. Tearney, and B. E. Bouma, Appl. Phys. Lett. **88**, 103902 (2006).
[28] C. Joo, K. H. Kim, and J. F. de Boer, Opt. Lett. **32**, 623 (2007).
[29] Y.-C. Ahn, W. Jung, and Z. Chen, Appl. Phys. Lett. **89**, 064109 (2006).
[30] K. Wiesauer, M. Pircher, E. Götzinger, C. K. Hitzenberger, R. Engelke, G. Grützner, G. Ahrens, R. Oster, and D. Stifter, Insight **49**, 275 (2007).
[31] S. G. Demos, M. Staggs, K. Minoshima, and J. Fujimoto, Opt. Express **10**, 1444 (2002).
[32] D. Stifter, K. Wiesauer, M. Wurm, E. Leiss, M. Pircher, E. Götzinger, B. Baumann, and C. K. Hitzenberger, in 17th World Conference on Nondestructive Testing, 2008, p. 17.
[33] D. Stifter, K. Wiesauer, M. Wurm, E. Schlotthauer, J. Kastner, M. Pircher, E. Götzinger, and C. K. Hitzenberger, Meas. Sci. Technol. **19**, 074011 (2008).
[34] B. R. Biedermann, W. Wieser, C. M. Eigenwillig, G. Palte, D. C. Adler, V. J. Srinivasan, J. G. Fujimoto, and R. Huber, Opt. Lett. **33**, 2556 (2008).
[35] K. Wiesauer, M. Pircher, E. Götzinger, S. Bauer, R. Engelke, G. Ahrens, G. Grützner, C. K. Hitzenberger, and D. Stifter, Opt. Express **13**, 1015 (2005).
[36] J. A. Izatt, M. R. Hee, and G. M. Owen, Opt. Lett. **19**, 590 (1994).
[37] M. C. Knauer, C. Richter, and G. Häusler, Laser J. **1**, 33 (2006).
[38] P. R. Herman, K. P. Chen, M. Wei, J. Zhang, J. Ihlemann, D. Schäfer, G.

Marowsky, P. Oesterlin, and B. Burghardt, Proc. SPIE **4274**, 149 (2001).
[39] J. Ihlemann, S. Müller, S. Puschmann, D. Schäfer, P. R. Herman, J. Li, and M. Wei, Proc. SPIE **4941**, 94 (2003).
[40] T. Fricke-Begemann, J. Li, J. Dou, J. Ihlemann, P. Herman, and G. Marowsky, Proceedings of the Third International WLT-Conference on Lasers in Manufacturing, 2005, p. 733.
[41] M. Born and E. Wolf, *Principles of Optics*, 6th ed. (University Press, Cambridge, 1997), pp. 370–458.
[42] P. H. Tomlins and R. K. Wang, J. Phys. D: Appl. Phys. **38**, 2519 (2005).
[43] P. E. Dyer, C. D. Walton, and K. A. Akeel, Opt. Lett. **30**, 1336 (2005).
[44] D. Schäfer, "Diffractive phase elements for partial coherent UV laser beams," Ph.D. thesis, Georg-August-Universität Göttingen, 2001.